

The Binding of Fe(II)–Heme to the Amyloid Beta Peptide of Alzheimer's Disease: QM/MM Investigations

Samira Azimi and Arvi Rauk*

Department of Chemistry, The University of Calgary, Calgary, Alberta, Canada T2N 1N4

S Supporting Information

ABSTRACT: The structures of complexes between $A\beta(1-42)$ and ferroheme (Fe(II)–heme) were determined by application of Amber and ONIOM(B3LYP/6-31G(d):Amber) methodology. Attachment at each of the three His residues was investigated. In each case, direct bonding of the iron to the His residue is augmented by the formation of secondary salt bridges between the carboxylate groups of the heme and positively charged residues of $A\beta$ (at His13, by Lys16 and the N-terminus; at His14, by both Lys16 and Lys28; at His6, by Arg5) or by H-bonding and hydrophobic interactions (at His6, by Asp7 or Phe20). The results indicate a slight preference for His13 followed by His6 and His14, with the lowest eight structures lying within 36 kJ mol⁻¹ of each other. The methodology is not precise enough to permit a definitive statement as to the relative stabilities, nor to the absolute binding affinities, which are predicted to be less than 70 kJ mol⁻¹. The results bear on the question of how heme and copper may bind simultaneously to $A\beta$. They confirm that the reduced species can bind independently, Cu⁺ at His13–His14 and Fe(II)–heme at His6.

INTRODUCTION

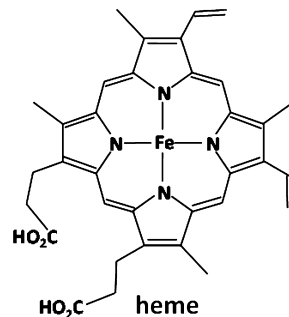
The pathological symptoms of Alzheimer's disease (AD) are a loss of neurons and synapses in the cerebral cortex, resulting in long- and short-term memory loss and disability in thinking and learning.¹ The physiological hallmarks are the appearance of intracellular tangles of an abnormal form of the tau protein and extracellular plaques consisting primarily of the amyloid beta peptide ($A\beta$) and with elevated levels of copper, zinc, and iron. Although the cause of AD is unknown, current consensus is that the neurotoxic agents are soluble oligomeric forms of $A\beta$, most likely associated with metal ions.

The sequence of $A\beta(1-42)$, in single letter code, is



The mechanisms of neuronal toxicity of $A\beta$ are complex and multifaceted, involving various reactive oxygen (radicals) species (ROS) that cause general inflammation and lipid peroxidation, as well as other effects such as interference with the proper functioning of insulin and glutamine receptors at synapses and a loss of calcium homeostasis. The association with metals accelerates oligomerization and, in the case of the redox active metals copper and iron, promotes ROS formation. It is this latter aspect, and iron specifically, that is the subject of the present study.

Free inorganic iron is very tightly regulated and is present in a negligibly low concentration. The relevant form of active iron is heme, the complex between Fe(III) or Fe(II) and protoporphyrin IX. Heme is a prosthetic group in numerous enzymes responsible for oxygen transport (hemoglobin) and redox activity (catalase, peroxidases, the cytochromes). Heme associates with the beta amyloid peptide and has peroxidase activity.² $A\beta$ has been shown to have two binding sites for heme, in the hydrophilic domain, residues 1–16, and in the



hydrophobic domain, residues 17–40/42. Spectroscopic evidence seems to suggest that ferriheme (Fe(III)–heme) and cupric ions (Cu²⁺) bind to $A\beta$ simultaneously and independently of each other.³ These observations seem to contradict what is accepted about the nature of the coordination of copper to $A\beta$. Numerous experimental and theoretical studies^{4–12} have shown that Cu²⁺ also binds in the hydrophilic domain, principally at the His residues and the N-terminus, while cuprous ion (Cu⁺) binds solely at His13 and His14. The complex pH-dependent nature of the Cu²⁺ binding has recently been clarified computationally on model systems.¹³ The lower pH component (component I) is associated with the N-terminus, His6, and either His13 or His14. At higher, more physiological pH, this component morphs into a second component (component II) that is bound to all three His residues as well as an amide carbonyl oxygen atom of Ala2.

In contrast, little is known about the nature of the binding of heme to $A\beta$.¹⁴ $A\beta$ lacks Cys residues so the attachment cannot be of the cytochrome P450 kind.¹⁵ $A\beta$ has a Tyr residue so the

Special Issue: Berny Schlegel Festschrift

Received: August 14, 2012

Published: September 12, 2012



binding could be of the catalase kind.¹⁶ However, the peroxidase-like activity argues against this and suggests that the heme should be attached to one of the three His residues,^{17,18} at positions, 6, 13, and 14, all of which have been shown experimentally and theoretically to serve as binding sites for Cu²⁺. There is almost universal agreement that His6 is involved in Cu²⁺ binding in both component I and component II of Cu(II)/A β . At least in the case of component I, either His13 or His14 could bind the heme and the other serve as a second ligand for the copper. However, it seems unlikely that the heme and Cu²⁺ could be bound independently to His13 and His14 since the two residues are in close proximity and some spectroscopic perturbation should be evident. The alternative, that His13 and His14 are reserved for the copper and that His6 is the heme-binding site, would call into question the experimental data that suggest His6 to be involved in the Cu²⁺ binding in both component I and component II. The Cu²⁺/A β complex also displays peroxidase activity: under reducing conditions in the presence of O₂, H₂O₂ is produced. The redox chemistry proceeds through the reduced forms of the metal complexes, ferroheme/A β (Fe(II)-heme-A β) and Cu⁺/A β , suggesting that the same His residue binds both the oxidized and reduced metals. If it is true that heme and Cu²⁺ bind simultaneously and independently, this puzzling result would require that all of the His residues not be simultaneously bound to Cu²⁺, and it begs the question as to which His residue coordinates the heme.

Atamna and co-workers have shown that Fe(III)-heme binds to A β with submicromolar affinity, implying that $\Delta G \approx -40$ kJ/mol.¹⁴ This result was supported in a recent computational study of the binding of imidazole to Fe(III) porphine (a model for heme), $\Delta G = -44$ kJ/mol.¹⁹ However, a substantially lower value was obtained for Fe(II)-heme, $\Delta G = -16$ kJ/mol.^{19,20} Peroxidase activity proceeds not through Fe(III)-heme-A β but rather through the reduced form, Fe(II)-heme-A β . Logically, electrostatic interactions between the two propylcarboxy groups and positively charged residues (N-terminus, Arg5, Lys16, or Lys28) should contribute to, and strengthen, the binding of the reduced heme to A β . The objective of the present study is to determine the structure and character of the binding of the peroxidase-active Fe(II)-heme to each His6, His13, and His14, to determine if there is a clear preference for the binding to one of the His residues, to attempt to determine the binding affinity, and to shed some light on the simultaneous copper-heme binding question.

METHODS

All calculations were carried out with the Gaussian 09 (G09) suite of programs.²¹ The bulk of the calculations on the complete A β -heme system were carried out with the Amber force field²² or using mixed quantum mechanical-molecular mechanical (QM/MM) methodology, ONIOM.^{23,24} Validation of the Amber part of the study was performed by comparison with pure B3LYP/6-31G(d) calculations on the part of the system that would become the "QM" part, namely the 4-methylimidazole (MeIm) complex with Fe(II)-heme. Accordingly, the geometries of MeIm, Fe(II)-heme in its triplet electronic state, and their adduct, also in the triplet state, were optimized at the B3LYP/6-31G(d) level of theory.²⁵ Harmonic frequency analysis was also conducted at the same level of theory in order to obtain zero-point vibrational energies, the entropy at 298 K, and thermal corrections to the enthalpy, also at 298 K. The zero point energy was scaled by 0.9806.²⁶ The

entropy at 1 atm of pressure was converted to a 1 M standard state by the addition of Rln(1/24.465). The free energy of solvation, ΔG_{solv} , was obtained via the SCRF keyword with the default parameters for water as implemented in G09.²⁷ In addition, the missing dispersion energy in B3LYP was estimated by the DFT-D3 procedure of Grimme and co-workers.²⁸

Geometries for each A β -heme complex were optimized initially by the Amber force field. It was necessary to define missing parameters for heme. The Amber charges for the atoms in Fe(II)-heme were taken as the NBO charges obtained from the B3LYP/6-31+G(d) wave function of the B3LYP/6-31G(d)-optimized geometry of the complex in its triplet state. A sample input file containing all of the parameters is included in the Supporting Information. The initial structure of A β was taken from the molecular dynamics study of Raffa and Rauk.²⁹ A search for the lower energy conformations of the heme moiety attached to each of the His residues was carried out as follows. In the first step, the heme was held at a fixed distance of 6 Å and rotated in 30° steps about the Fe-N^e(His) bond with complete geometry optimization by Amber. For each of the torsional minima, the Fe-N distance was reduced in steps of 1 Å with complete reoptimization at each step, down to a distance of 3 Å, and a final distance of 2.4 Å. It was hoped that this "annealing" procedure would allow both the heme and the A β moieties to settle into the energetically most favorable orientations. In many cases, manual intervention was applied to move some side chains, particularly of Lys and Arg residues, into positions that either would avoid too-close-proximity clashes or might permit the formation of salt bridges. Of the several hundred structures thus optimized, approximately 20 of the lowest energy conformations of each of His6-, His13-, and His14-bound structures were selected for complete QM/MM optimization. In G09, the QM/MM implementation is ONIOM. Optimization of each structure was invoked with the command, "ONIOM(B3LYP/6-31G(d): AMBER=hard-first) = embedcharge". The "QM" part of the system corresponds to the Fe(II)-heme and the side chain of each His residue, converted into MeIm by the addition of a hydrogen to the β -C and linked mechanically to the α -C. The "embedcharge" keyword denotes that the Amber charges are seen by the "QM" system. With such a large system (85 atoms in the QM part, 700 atoms in A β -heme), it was not feasible to perform harmonic frequency analysis on all of the structures, and so zero point energies and thermal corrections were determined for the 30 lowest energy species. The effect of implicit solvation by water was included at the IEFPCM level as described above.²⁴ The dispersion part of the total energy missing from the B3LYP treatment of the QM part was estimated by the DFT-D3 procedure²⁸ and added to the total energy.

RESULTS

The Structure of A β (1-42). There are a number of A β structures deposited in the Brookhaven Protein Data Bank. However, these were not deemed suitable for the present study as they were derived from NMR data obtained not in water but under helix-forcing conditions. Our original structure for A β (1-42) was taken from a Gromacs MD simulation in water—the structure evolved after 350 ns, and no further change occurred for the next 1000 ns, indicating that it is stable for at least 1 μ s.²⁹ This structure was reoptimized in the gaseous phase with the Amber force field implemented in G09. Despite

the differences in the environment and the force field, the reoptimized structure differs from the original by only RMSD = 0.86 Å (Figure 1). The structure is roughly spherical in shape

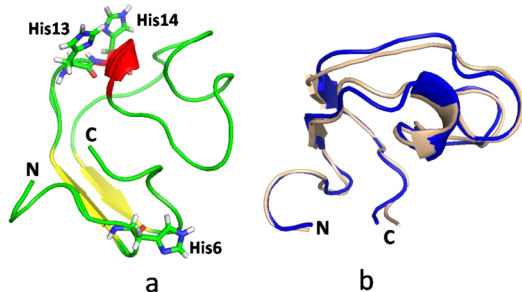


Figure 1. (a) Cartoon of Amber-optimized $\text{A}\beta$ (1–42). (b) Superposition of the Amber-optimized structure (blue) and the structure of Raffa and Rauk, ref 29 (creamy white). The orientation has been rotated about 90° about a horizontal axis from part a.

with the N and C termini in close proximity. It has an antiparallel β sheet between residues Ser8–Tyr10 and Leu34–Val36, a short α -helical segment formed by residues His14–Lys16, and a loose helical coil spanning Glu22–Gly29. There are also β strands spanning residues Lys16–Phe20 and Gly37–Val40, which are not close enough to be identified by the software as a β sheet. The possible binding sites for heme, His6, His13, and His14, are on the surface and available for binding of both heme and Cu(II) or Cu(I).

The Structure of Fe(II)–Heme. Heme is a complex between the iron ion and protoporphyrin IX. The distinguishing features of the ferrous form are the central Fe(II) ion and two propylcarboxy groups which give the overall complex a charge of −2. The structure of Fe(II)–heme, reoptimized with the Amber force field in the gaseous phase, differs little from that optimized at the B3LYP/6-31G(d) level in the gaseous phase. This, together with the above-mentioned results on $\text{A}\beta$ itself, suggests that the Amber force field should be suitable for the preliminary structural studies of the $\text{A}\beta$ –heme system used to select the most stable complexes for QM/MM optimization.

The Structure and Energetics of Fe(II)–Heme–4-Methylimidazole (the “QM” Part). 4-Methylimidazole (MeIm) is a model for the side chain of the His residues. Coordination of imidazole to Fe(II)–heme is very weak, $\Delta G \approx -20 \text{ kJ mol}^{-1}$.^{19,30,31} In the B3LYP/6-31G(d)-optimized

structure, the Fe–N^e separation is 2.304 Å. The Fe(II)–heme–MeIm system is small enough so that all of the steps required to calculate the free energy of dissociation in water at 298 K can be carried out. These include B3LYP/6-31G(d) optimization, harmonic frequency analysis, solvation correction by IEFPCM, and dispersion correction by DFT-D3. The primary data are given in Table 1, and the data for the reaction between the heme and MeIm are listed in Table 2. The free energy of binding of MeIm to Fe(II)–heme at 298 K in water is calculated to be $\Delta G = -10 \text{ kJ mol}^{-1}$, in reasonable agreement with experimental values and previous ab initio calculations on model systems.²⁰ We conclude from these results that the approximate methodology that must be applied, namely QM/MM (B3LYP/6-31G(d)/Amber), with solvation, thermal, and dispersion corrections, is adequate to describe the Fe(II)–heme– $\text{A}\beta$ system.

Structures of Fe(II)–Heme Bound to $\text{A}\beta$ at His6, His13, and His14. Table S1 of Supporting Information lists all of the primary computed energy data as well as key structural information for the 19 isomers of the Fe(II)–heme– $\text{A}\beta$ system which had relative aqueous free energy under 100 kJ mol^{−1}, in decreasing order of stability. The last column indicates the root-mean-square deviation (RMSD) of all of the atoms of the $\text{A}\beta$ backbone of the Amber-optimized structure, and the ONIOM-optimized structure. All of the RMSD values are within 2 Å, indicating that there is no major change in the $\text{A}\beta$ conformation upon attachment of the heme, regardless of where the heme is attached. This is illustrated graphically in Figure 2 where the Amber-optimized $\text{A}\beta$ structure (pale cream) is compared to the ONIOM-optimized structure (blue) in cartoon representation. The lowest energy complex of each type is shown. The most stable structure, Fe(II)–heme– $\text{A}\beta$ (H13)a, is one in which the heme is attached to His13. It is approximately 24 kJ mol^{−1} more stable than the lowest His6-bound system, Fe(II)–heme– $\text{A}\beta$ (H6)a, and 31 kJ mol^{−1} lower than the His14-bound complex, Fe(II)–heme– $\text{A}\beta$ (H14)a. Two more His13-bound structures, Fe(II)–heme– $\text{A}\beta$ (H13)b and Fe(II)–heme– $\text{A}\beta$ (His13)c, are similar in energy to Fe(II)–heme– $\text{A}\beta$ (H6)a, as is a second His6-bound one, Fe(II)–heme– $\text{A}\beta$ (H6)b. In all, eight structures lie in the range 24–40 kJ mol^{−1}. In view of the approximations in the methodology, structures that lie within about 20 kJ mol^{−1} of each other should be taken as equally probable.

Table 1. Calculated Data for Fe(II)–heme (heme), 4-Methylimidazole (MeIm), and the Complex (heme–MeIm, the QM part), $\text{A}\beta$ (1–42), and Fe(II)–heme– $\text{A}\beta$ Complexes

molecule	energy ^a hartree	ZPVE hartree	$H_{298}^\circ - H_0^\circ \text{ kJ mol}^{-1}$	$S_{298} \text{ J k}^{-1} \text{ mol}^{-1}$	disp kJ mol^{-1}	$\Delta G_{\text{solv}} \text{ kJ mol}^{-1}$	$\Delta G(\text{aq}) \text{ kJ mol}^{-1}$
heme	−3097.35069	0.57051	107.2	999.8	−246.4	−636.3	
MeIm	−265.53543	0.09923	16.7	281.7	−13.6	−27.3	
heme–MeIm	−3362.90544	0.67056	126.4	1162.2	−297.3	−635.5	
Fe(II)–heme– $\text{A}\beta$ (H13)a	−3364.62912	5.80390	962.3	6947.9	−308.9	−2091.5	0.0
Fe(II)–heme– $\text{A}\beta$ (H14)a	−3364.60378	5.80368	960.8	6927.9	−308.4	−2131.4	28.2
Fe(II)–heme– $\text{A}\beta$ (H6)a	−3364.58845	5.80070	965.5	7004.5	−293.6	−2163.3	31.0
$\text{A}\beta$ (H13)	−267.30253 ^b	5.22760	853.9	6170.4	−13.6	−1197.1	92.1
$\text{A}\beta$ (H6)	−267.35742 ^b	5.22862	856.7	6176.0	−13.6	−1148.9	0.0
$\text{A}\beta$ (H14)	−267.33523 ^b	5.23190	852.9	6154.8	−13.6	−1171.8	46.5
$\text{A}\beta$ _{13Amber}	−267.30185 ^c	5.22445	861.8	6263.3	−13.6	−1248.1	14.8
$\text{A}\beta$ _{6Amber}	−267.30007 ^c	5.22424	861.9	6273.6	−13.6	−1261.8	2.2
$\text{A}\beta$ _{14Amber}	−267.30149 ^c	5.22510	860.4	6247.8	−13.6	−1259.7	9.2

^aGaseous phase. ^bOptimized from structure of complex. ^cOptimized from Amber-optimized $\text{A}\beta$.

Table 2. Reaction Energies (kJ mol^{-1})^a

reaction	ΔE	ΔZPVE	ΔDisp	ΔH_0	ΔH_{298}	$-T\Delta S$	$\Delta G_{(\text{gas})}$	$\Delta \Delta G_{\text{solv}}$	$\Delta G_{(\text{aq})}$
heme–MeIm \Rightarrow heme + MeIm	50.7	−2.2	37.3	86.0	83.4	−35.6	47.8	−38.0	9.8
$-\text{A}\beta(\text{H13})\text{a} \Rightarrow \text{eq 1a}$	−207.4	−12.9	48.8	−170.8	−169.2	−68.0	−237.2	306.3	69.1
$-\text{A}\beta(\text{H6})\text{a} \Rightarrow \text{eq 1b}$	−272.4	−4.0	33.5	−242.9	−244.5	−51.1	−295.6	336.4	40.8
$-\text{A}\beta(\text{H14})\text{a} \Rightarrow \text{eq 1c}$	−273.9	−11.7	48.4	−237.3	−234.1	−73.9	−308.0	346.2	38.1

^a ΔE = Born–Oppenheimer; ΔDisp = dispersion correction; ΔH_0 , ΔH_{298} = enthalpy at 0 and 298 K; ΔS = entropy at 298 M and 1 M; $\Delta G_{(\text{gas})}$, $\Delta G_{(\text{aq})}$ = Gibbs free energy in gaseous and aqueous phases; $\Delta \Delta G_{\text{solv}}$ = free energy of solvation.

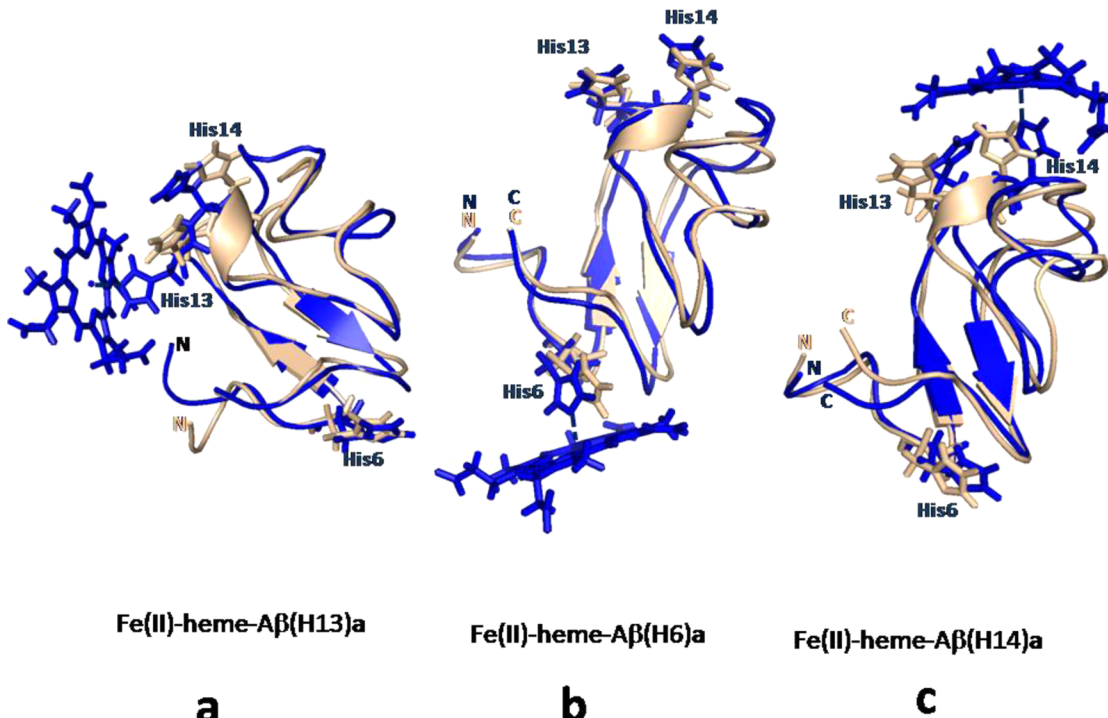


Figure 2. Cartoon representations of the Amber-optimized $\text{A}\beta(1-42)$ (creamy white) superimposed on the three most stable ONIOM-optimized structures of complexes (blue): (a) $\text{Fe}(\text{II})-\text{heme}-\text{A}\beta(\text{H13})\text{a}$; (b) $\text{Fe}(\text{II})-\text{heme}-\text{A}\beta(\text{H6})\text{a}$; (c) $\text{Fe}(\text{II})-\text{heme}-\text{A}\beta(\text{H14})\text{a}$.

The explicit heme bonding details of the eight lowest energy structures are shown in Figures 3–5. In the most stable structure, $\text{Fe}(\text{II})-\text{heme}-\text{A}\beta(\text{H13})\text{a}$ (Figure 3), the short $\text{Fe}-\text{N}^e$ separation, 2.30 Å (Table S1), indicates coordination of the Fe to N^e of His13. Only one of the propylcarboxylate groups of the heme is involved in salt bridges. The side chain of Lys16 has extended to reach it. Significant displacements of the N terminus and the side chain of His13 with its pendant heme have brought the two moieties close enough to make a second salt bridge to the same heme carboxylate. The displacement of the N terminus is evident in the cartoon representations in Figure 2a. The same bonding and salt bridge configuration as $\text{Fe}(\text{II})-\text{heme}-\text{A}\beta(\text{H13})\text{a}$ is present in the second structure, $\text{Fe}(\text{II})-\text{heme}-\text{A}\beta(\text{H13})\text{b}$ (Figure 3 inset), 24 kJ mol^{-1} higher than the first, and in $\text{Fe}(\text{II})-\text{heme}-\text{A}\beta(\text{His13})\text{c}$ (not shown). $\text{Fe}(\text{II})-\text{heme}-\text{A}\beta(\text{H13})\text{b}$ differs mainly in a different configuration of the Lys16 side chain which in $\text{Fe}(\text{II})-\text{heme}-\text{A}\beta(\text{H13})\text{a}$ is completely staggered but in $\text{Fe}(\text{II})-\text{heme}-\text{A}\beta(\text{His13})\text{b}$ has a number of gauche orientations along the chain (the RMSD of the backbone is 1.09 Å). In $\text{Fe}(\text{II})-\text{heme}-\text{A}\beta(\text{His13})\text{c}$, the C-terminal carboxylate has also folded over to make a competing salt bridge with Lys16.

The two lowest energy structures in which the heme is attached to His6, $\text{Fe}(\text{II})-\text{heme}-\text{A}\beta(\text{H6})\text{a}$ and $\text{Fe}(\text{II})-\text{heme}-\text{A}\beta(\text{H6})\text{b}$, at 28 and 33 kJ mol^{-1} , are shown in Figure 4. They

have essentially the same energy as several His14-bound structures (see below). In $\text{Fe}(\text{II})-\text{heme}-\text{A}\beta(\text{H6})\text{a}$ (Figure 4a), neither carboxylate of the heme is involved in salt bridging. The bonding appears to be entirely through the His6–Fe coordination. The close proximity between Phe20 and a methyl and vinyl group of the heme may be indicative of a secondary hydrophobic bonding interaction. The heme binding configuration of $\text{Fe}(\text{II})-\text{heme}-\text{A}\beta(\text{H6})\text{b}$ (Figure 4b) is quite different. His6 is attached to the iron, and one of the carboxylate groups is exposed to the solvent while the other makes a H bond to the amide $\text{N}-\text{H}$ of His6. His6 is too far from Lys16 and Lys28 to become involved in salt bridges to the heme. One notes that Arg salt bridging to heme is a common theme in heme proteins,³² but in neither of the two lowest energy His6-bound structures is Arg5 involved. In both structures, the arginine makes salt bridges to Glu3 and Asp7, more clearly seen in Figure 4b. The lowest energy structure in which Arg5 is involved is $\text{Fe}(\text{II})-\text{heme}-\text{A}\beta(\text{H6})\text{e}$ (Figure 4 inset), 25 kJ mol^{-1} higher than $\text{Fe}(\text{II})-\text{heme}-\text{A}\beta(\text{H6})\text{a}$. Here, Arg5 makes salt bridges to both heme carboxylate groups but in doing so drags the heme group away from His6. The $\text{Fe}-\text{N}^e$ distance, 3.99 Å, is too great for His6 coordination to the iron. Instead, His6 makes a H bond to Asp7.

The lowest energy His14-bound structure, $\text{Fe}(\text{II})-\text{heme}-\text{A}\beta(\text{H14})\text{a}$ (Figure 4a), is 31 kJ mol^{-1} higher in energy than

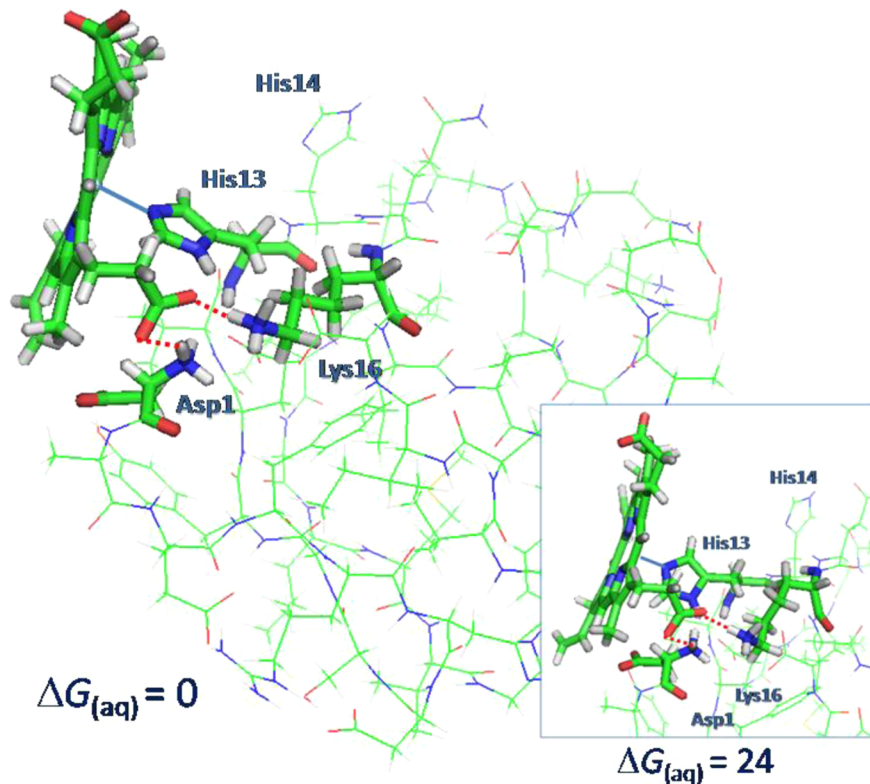


Figure 3. ONIOM-optimized structures of Fe(II)–heme–A β (H13)a and Fe(II)–heme–A β (H13)b (inset) showing details of the bonding environment of the heme. The heme group and the side chain of His13 constitute the QM part. $\Delta G_{(aq)}$ is relative to Fe(II)–heme–A β (H13)a in kJ mol $^{-1}$.

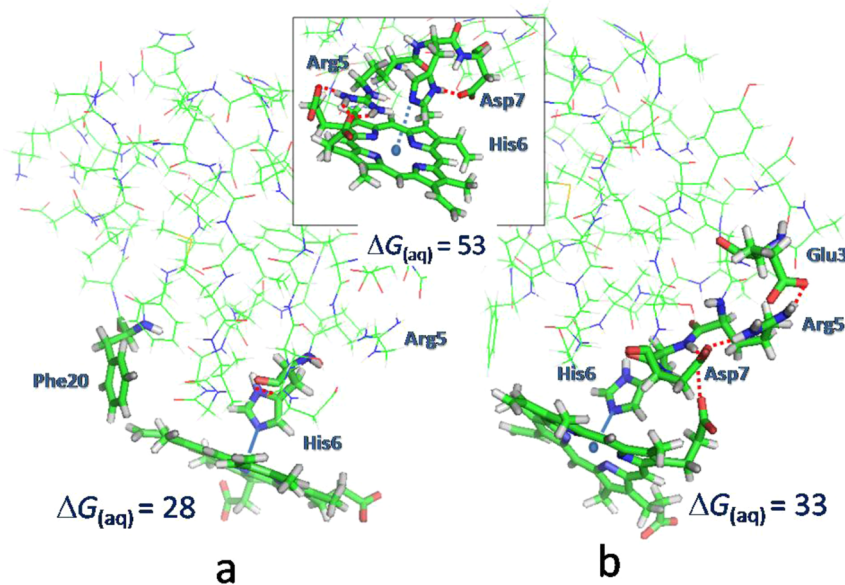


Figure 4. ONIOM-optimized structures of His6-bound heme showing details of the bonding environment of the heme: (a) Fe(II)–heme–A β (H6)a; (b) Fe(II)–heme–A β (H6)b; (inset) Fe(II)–heme–A β (H6)e. The heme group and the side chain of His6 constitute the QM part. $\Delta G_{(aq)}$ is relative to Fe(II)–heme–A β (H13)a in kJ mol $^{-1}$.

Fe(II)–heme–A β (H13)a. It has a slightly longer Fe–N e separation, 2.32 Å (Table S1). Both propylcarboxylate groups of the heme are involved in salt bridges. As in the case of Fe(II)–heme–A β (H13)a, the side chain of Lys16 has extended to reach one of the carboxylate groups. Additional bonding to this carboxylate accrues from H bonds to Gln15 and Asn28. The second carboxylate group makes a salt bridge with Lys28.

As can be seen in the cartoon representations in Figure 2b, the N-terminal chains and the side chain of His13 are hardly perturbed by the attachment of the heme to His14, but there is significant perturbation at the C terminus and at midchain. However, both His13 and His14 side chains have been displaced as a result of the binding. The bonding motif in Fe(II)–heme–A β (H14)c (5 kJ mol $^{-1}$ higher) is similar in that

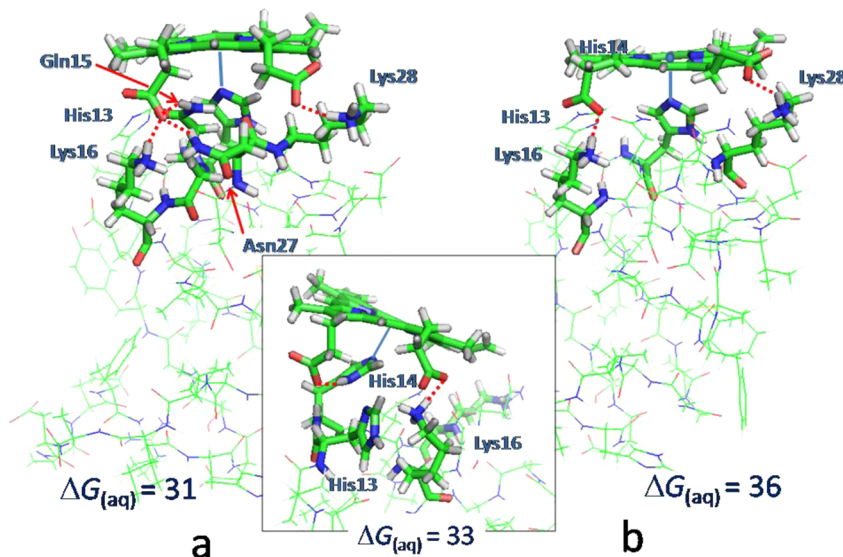
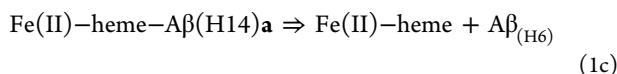
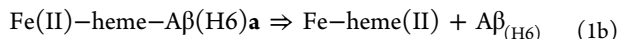
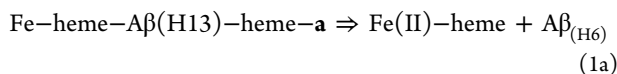


Figure 5. ONIOM-optimized structures of (a) Fe(II)-heme- $A\beta$ (H14)a; (b) Fe(II)-heme- $A\beta$ (H14)c; (inset) Fe(II)-heme- $A\beta$ (H14)b showing details of the bonding environment of the heme. The heme group and the side chain of His14 constitute the QM part. $\Delta G_{(aq)}$ is relative to Fe(II)-heme- $A\beta$ (H13)a in kJ mol^{-1} .

both heme carboxylate groups are interacting with Lys16 and Lys28, but additional interactions with Gln15 and Asn27 are not evident. The bonding configuration of Fe(II)-heme- $A\beta$ (H14)b, which lies between the others, is shown as the inset to Figure 5. In this case, one of the heme carboxylate groups has H-bonded to imidazole N-H of His14 and pulled it away from the ideal perpendicular orientation. Its low energy, similar to the other His14-bond structures, ensues from an unusually large stabilization from the dispersion term. This may be due to increased π -stacking, a consequence of the tilt of the plane of the imidazole group toward the heme plane.

Binding Affinity of Fe(II)-Heme Bound to $A\beta$ at His6, His13, and His14. The binding affinity of ferroheme to $A\beta$ was assessed by calculating the energy changes for reactions 1a–1c:



The data for the heme/ $A\beta$ complexes was taken from Table S1, and those for Fe(II)-heme (heme) are listed in Table 1. In the reactions, the QM part is separated, requiring ONIOM calculations on $A\beta$ with each of the His side chains defined as the QM part. Each “ $A\beta$ ” structure, $A\beta_{(\text{H13})}$, $A\beta_{(\text{H6})}$, and $A\beta_{(\text{H14})}$, which represents the conformation of $A\beta$ after detachment of the heme, was separately ONIOM-optimized in the same way as the whole complex and subjected to single point solvation. The optimizations should yield the closest energy minimum to the corresponding heme-bound structure. As a result, the relative aqueous free energies of $A\beta_{(\text{H13})}$, $A\beta_{(\text{H6})}$, and $A\beta_{(\text{H14})}$ are different from each other (kJ mol^{-1}): $A\beta_{(\text{H13})}$, 92.1; $A\beta_{(\text{H6})}$, 0.0; $A\beta_{(\text{H14})}$, 46.5. As a separate test of the reproducibility of the ONIOM mechanical and charge embedding methodology, each of the His residues in the *Amber*-optimized $A\beta$ structure (Figure 1) was made into the QM part and the entire system ONIOM-

optimized. Ideally, each of these three tests should yield the same ONIOM energy in the gas phase and after solvation. The test “ $A\beta$ ’s” are labeled $A\beta_{13\text{Amber}}$, $A\beta_{6\text{Amber}}$, and $A\beta_{14\text{Amber}}$ in Table 1. In the gas phase, the relative free energies were (kJ mol^{-1}): $A\beta_{13\text{Amber}}$, 0.0; $A\beta_{6\text{Amber}}$, 5.9; $A\beta_{14\text{Amber}}$, 1.2. In aqueous solution, the relative free energies were (kJ mol^{-1}): $A\beta_{13\text{Amber}}$, 12.6; $A\beta_{6\text{Amber}}$, 0.0; $A\beta_{14\text{Amber}}$, 9.2. Thus, the reproducibility in the gas phase is reasonably good, with a spread of less than 6 kJ mol^{-1} . It is less so in solution where the difference is more than 12 kJ mol^{-1} . One notes that the absolute value of the free energy of solvation ΔG_{solv} , taken as the difference in the SCRF energy and gaseous phase energy, is much larger (kJ mol^{-1}): $A\beta_{13\text{Amber}}$, -1248.1; $A\beta_{6\text{Amber}}$, -1261.8; $A\beta_{14\text{Amber}}$, -1259.7. The largest $\Delta\Delta G_{\text{solv}}$ is almost 14 kJ mol^{-1} .

The data for the calculation of the binding affinities according to eqs 1a–1c, are given in Table 1. Table 2 provides the computed details for the reactions. Each complex is taken as dissociating into Fe(II)-heme and $A\beta_{(\text{H6})}$, the lowest in energy of the ONIOM $A\beta$ results. One can see from the column ΔH_0 or $\Delta G_{(\text{gas})}$ of the last three rows of Table 2 that none of the complexes are predicted to be stable in the gaseous phase. This is not unexpected because of the high charge of the system, $-5e$, assembled from $A\beta$ with a charge of $-3e$ and Fe(II)-heme with charge of $-2e$. The zero point vibrational energy, $\Delta ZPVE$, makes about 13 kJ mol^{-1} difference, much more than expected as judged by the heme-MeIm \Rightarrow heme + MeIm reaction (Table 2). There is a large difference in the dispersion correction for the three reactions. The change in free energy of solvation, $\Delta\Delta G_{\text{solv}}$, is large and positive and more than compensates for the gaseous phase repulsion. The predicted binding energy, $\Delta G_{(\text{aq})}$, of the most stable structure, Fe(II)-heme- $A\beta$ (H13)a, is 69 kJ mol^{-1} . This is in qualitative agreement with the value of Atamna et al. for the binding of Fe(III)-heme to $A\beta$, 40 kJ/mol ,¹⁴ but not of Fe(II)-heme or Fe(II)-porphine to imidazole, 16 kJ mol^{-1} .^{19,20}

DISCUSSION

In this preliminary investigation of the interactions of heme with $A\beta$, we chose to study the reduced ferroheme (Fe(II))–

heme) because it is the redox active form. We asked whether it would be possible to determine computationally at which of the three histidine residues the heme may be attached, what bonding configurations can arise at the different sites, and whether the binding affinity could be determined. Out of necessity, because of the large size of the system (700 atoms), geometry optimization had to be carried out in the gaseous phase, a far from optimum situation for a system with such a high charge ($-5e$). Hundreds of initial interactions between the empirical solution structure of $\text{A}\beta(1-42)$ and $\text{Fe}(\text{II})-\text{heme}$ at each of the three His residues were examined by MM (Amber) minimization. Then, approximately 50 lowest energy structures were subjected to more detailed study. QM/MM methodology (ONIOM) was required in order to account properly for the spin state and electron distribution for the heme-imidazole bonding. The large QM region (85 atoms) required a fairly modest ab initio approach, B3LYP/6-31G(d). Because the ONIOM methodology cancels out the MM energy component of the QM part, the dispersion contribution to the energy inherent in the MM (Amber) force field was also subtracted out and needed to be replaced. In previous publications on smaller model systems, this deficiency of B3LYP was compensated for by single-point MP2/6-31G(d) calculations.^{13,19,20} However, in the present system, it was not possible to coax the MP2 calculation to converge reliably to the lowest energy triplet state of the $\text{Fe}(\text{II})-\text{heme}-\text{A}\beta$ system, and so it had to be abandoned. Instead, the empirical DFT-D3 procedure of Grimme was applied to the QM region to replace the missing dispersion term.²⁸ Single point harmonic frequency analysis permitted the derivation of zero point energy corrections and estimation of thermal effects. Finally, the effect of solvation on the total energy was estimated by applying the IEFPCM procedure to the system, as implemented in Gaussian 09.

The first consideration for the present study was the choice of structure for $\text{A}\beta(1-42)$ itself. We opted for the structure from Raffa and Rauk²⁹ which resulted from a Gromacs MD simulation in explicit water at 300 K. This structure evolved after about 350 ns and was stable for more than 1000 ns. Reoptimization in the gaseous phase did not substantively change its features. Neither did reoptimization with or without the heme attached by QM/MM (B3LYP/Amber). We deem this structure to be representative of the major conformation of $\text{A}\beta$ in solution and therefore suitable for examining various binding scenarios for the heme moiety.

Several distinct bonding motifs emerged. At His13, the attachment of the iron atom to the imidazole was augmented by formation of salt bridges between one of the heme carboxylate groups and the N terminus and Lys16 (Figure 3). Two distinct patterns emerged when the heme approached His6. Either the carboxylates were involved in salt bridges or they were not. In the latter case, additional bonding ensued from a hydrophobic interaction between the side chain of Phe20 and a peripheral methyl and vinyl group of the heme (Figure 4a). One of the carboxylate groups formed a H bond with an amide N-H bond (Figure 4b) or a salt bridge to Arg5 (Figure 5 inset). Unexpectedly, the interaction with Arg5 pulled the heme away from His6, yielding a relatively unstable configuration. At His14, as well as formation of a bond between iron and imidazole, salt bridges formed between Lys16 and Lys28 to the carboxylates in two of the three most stable structures (Figure 5a,b). In one case, one of the carboxylates made a H bond to the N^δ -H of His14, causing it to tilt out of the ideal perpendicular orientation for coordination. This

distortion toward incipient π -stacking was accompanied by an unusually large dispersion correction.

A structure, $\text{Fe}(\text{II})-\text{heme}-\text{A}\beta(\text{His}13)\text{a}$, in which the heme is attached to His13, emerged as the most stable structure by a small margin, 28 kJ mol^{-1} , over $\text{Fe}(\text{II})-\text{heme}-\text{A}\beta(\text{His}6)\text{a}$ (Figure 4 and Table S1). Two other structures, $\text{Fe}(\text{II})-\text{heme}-\text{A}\beta(\text{His}13)\text{b}$ and $\text{Fe}(\text{II})-\text{heme}-\text{A}\beta(\text{His}13)\text{c}$, were predicted to be more stable, by 3 and 5 kJ mol^{-1} . Because of the nature of the approximations in the model chemistry, it is not possible to say with certainty which of the His residues preferentially binds the heme. The same uncertainty pertains to the calculated binding energies. These were calculated for the most stable structure of each type. $\text{Fe}(\text{II})-\text{heme}-\text{A}\beta(\text{His}13)\text{a}$ is predicted to be bound by 69 kJ mol^{-1} (Table 2), a value in qualitative agreement with the experimental value for $\text{Fe}(\text{III})-\text{heme}-\text{A}\beta(1-42)$, 40 kJ mol^{-1} . However, the binding affinity for $\text{Fe}(\text{II})-\text{heme}$ is expected to be lower than for $\text{Fe}(\text{III})-\text{heme}$, in the vicinity of 16 kJ mol^{-1} based on calculations on $\text{Fe}(\text{II})-\text{porphine-imidazole}$.^{19,20}

So which His residue of $\text{A}\beta$ could be the attachment point for a heme? The energetic considerations point to His13, with His6 as the next possibility, and His14 a close third. We note from inspection of Figure 2 that His13 and His14 are well separated when the heme is attached to one or the other, but they are in close proximity when the heme is coordinated to His6. These considerations bear on the possible independent coordination of Cu^{2+} and Cu^+ together with heme as suggested by the detailed study by Pramanik et al.³ If the copper were coordinated only by a single His residue, then all of the lowest energy structures could bind the Cu and heme essentially independently. However, this is not the case. Although they differ in details, all of the numerous experimental studies of Cu^{2+} binding to $\text{A}\beta$ suggest at least two points of attachment to His residues, and most studies have His6 as one of them. Thus, His6 could be ruled out as a point of attachment of the heme in favor of His13 or His14, and the Cu^{2+} ion could be accommodated by the present model if it would attach to and stabilize the lower pH component I where only one, His13 or His14, is coordinated to the copper. In component I, by general agreement, the N terminus is also coordinated to the copper and not available for salt bridge formation to the heme if it were attached to His13. Thus, the heme should be attached to His14, the least stable configuration in the absence of copper. The preceding discussion assumes that attachment of $\text{Fe}(\text{III})-\text{heme}$ would be the same as that of the $\text{Fe}(\text{II})-\text{heme}$ of the present study. This is a reasonable assumption based on parallel theoretical studies of ligand binding to $\text{Fe}(\text{III})$ ¹⁹ and $\text{Fe}(\text{II})$ ²⁰ porphine complexes. However, the coordination pattern of Cu^{2+} is significantly different from that of Cu^+ . In $\text{A}\beta$, Cu^+ is coordinated in a linear fashion to the N^δ of both His13 and His14, a configuration that is only possible if the heme is attached at His6, as in the second most stable structure, $\text{Fe}(\text{II})-\text{heme}-\text{A}\beta(\text{His}6)\text{a}$. The seemingly contradictory experimental results vis a vis $\text{Fe}(\text{III})-\text{heme}$ and Cu^{2+} could be reconciled if the species whose spectroscopic signatures were being measured was not $\text{A}\beta/\text{Cu}/\text{heme}$ but rather a mixture of $\text{A}\beta/\text{heme}$ and $\text{A}\beta/\text{Cu}$. This is a reasonable conjecture since the binding affinities of $\text{Fe}(\text{III})-\text{heme}$ and Cu^{2+} for $\text{A}\beta$ are similar, $1.4 \times 10^{-7} \text{ M}^{14}$ and $0.6 \times 10^{-7} \text{ M}^{33}$, respectively.

Coordination of a His residue to the heme is a requirement to achieve the appropriate reduction potential for peroxidase activity, -0.3 V .²⁰ Thus, all of the lowest energy structures may do so. The $\text{A}\beta/\text{Cu}^{2+}$ complex can also function as a peroxidase.³

When separate equivalent amounts of $\text{A}\beta(1-16)/\text{Fe}(\text{III})-\text{heme}$ and $\text{A}\beta(1-16)/\text{Cu}^{2+}$ were reduced and exposed to air, equivalent stoichiometric amounts ($\approx 90\%$) of H_2O_2 were produced. The source of the second electron necessary for the reduction of O_2 to H_2O_2 was probably Tyr10. When the putative $\text{A}\beta(1-16)/\text{Fe}(\text{III})-\text{heme}/\text{Cu}^{2+}$ complex was treated in the same way, more than stoichiometric ($\approx 130\%$) amounts of H_2O_2 were produced.³ We suggest that this result is evidence that a 1:1:1 complex of the *reduced* metal species is indeed formed. While the affinity of $\text{Fe}(\text{II})-\text{heme}$ for $\text{A}\beta$ is not known, it is likely to be less than that of $\text{Fe}(\text{III})-\text{heme}$, i.e., $> 1.4 \times 10^{-7} \text{ M}^{14}$ due to the more negative charge of $\text{Fe}(\text{II})-\text{heme}$ and its inherently lower affinity for imidazole. On the other hand, the affinity of Cu^+ for $\text{A}\beta(1-16)$ is significantly *higher* than that of Cu^{2+} , $1 \times 10^{-14} \text{ M}^{34}$. Since Cu^+ is known to bind to both His13 and His14,³⁵ the $\text{Fe}(\text{II})-\text{heme}$ has uncontested access to His6. In the context of the present study, the candidate structure for $\text{Fe}(\text{II})-\text{heme}$ binding to $\text{A}\beta$ is $\text{Fe}(\text{II})-\text{heme}-\text{A}\beta(\text{His6})\text{a}$. Although it is not the most stable complex (Figures 3–5), it is the only candidate after Cu^+ is introduced.

CONCLUSIONS

The structures of complexes between $\text{A}\beta(1-42)$ and ferroheme ($\text{Fe}(\text{II})-\text{heme}$) were determined by application of QM/MM theoretical methodology, specifically ONIOM(B3LYP/6-31G-(d):Amber). Attachment at each of the three His residues was investigated. The results indicate a preference for His13 followed by His6 and His14. The lowest five structures shown in Figures 3–5 were all within 35 kJ mol⁻¹ of each other. The methodology is not precise enough to permit a definitive statement as to the relative stabilities, nor to the absolute binding affinities. It is likely that the ferroheme would be distributed among the three His residues in the absence of Cu^+ . In each case, direct bonding of the iron to the His residue is augmented by formation of secondary salt bridges between the carboxylate groups of the heme and positively charged residues of $\text{A}\beta$ (at His13, by Lys16 and the N-terminus; at His14, by both Lys16 and Lys28) or by a combination of H-bonding and hydrophobic interactions (at His6, by Asp7 or Phe20). The multipoint attachment may stabilize a nonamyloidogenic conformation and reduce the formation of neurotoxic oligomers and fibrils.

The present study cannot resolve the apparent contradictory assertions in the literature as to the nature of binding of ferriheme ($\text{Fe}(\text{III})-\text{heme}$) to $\text{A}\beta$ in the presence of Cu^{2+} . These on the one hand assert that ferriheme and Cu^{2+} can bind simultaneously and independently to $\text{A}\beta$ and on the other hand indicate that Cu^{2+} coordinates to at least two and probably all three His residues, leaving no room for the heme to attach in a fashion that would not perturb the Cu^{2+} coordination. On the other hand, our results confirm that the reduced species *can* bind independently, Cu^+ at His13–His14 and ferroheme at His6.

A study to examine the $\text{Fe}(\text{III})-\text{heme}/\text{A}\beta$ interactions is underway.

ASSOCIATED CONTENT

Supporting Information

Table S1 lists calculated data for 19 of the lowest energy $\text{Fe}(\text{II})-\text{heme}-\text{A}\beta(1-42)$ structures. The complete Gaussian 09 input file for ONIOM optimization of $\text{Fe}(\text{II})-\text{heme}-\text{A}\beta(\text{H13})\text{a}$ is also provided. The coordinates are for the optimized structure. This information is available free of charge

via the Internet at <http://pubs.acs.org>. Coordinates of the other structures are available from the authors by request.

AUTHOR INFORMATION

Corresponding Author

*E-mail: rauk@ucalgary.ca.

Notes

The authors declare no competing financial interest.

ACKNOWLEDGMENTS

We are grateful to the Natural Sciences and Engineering Research Council of Canada (NSERC) for financial support of this work and to Compute Canada and Westgrid for generous allocations of computational resources. We also thank Tebikie Wondimagegn for preliminary computational studies.

REFERENCES

- (1) An overview of the biochemistry of Alzheimer's disease is available at http://en.wikipedia.org/wiki/Biochemistry_of_Alzheimer's_disease (accessed September 2012).
- (2) Atamna, H.; Boyle, K. *Proc. Natl. Acad. Sci. U. S. A.* **2006**, *103*, 3381–3386.
- (3) Pramanik, D.; Ghosh, C.; Dey, S. G. *J. Am. Chem. Soc.* **2011**, *133*, 15545–15552.
- (4) Karr, J. W.; Akintoye, H.; Kaupp, L. J.; Szalai, V. A. *Biochemistry* **2005**, *44*, 5478–5487.
- (5) Faller, P.; Hureau, C. *Dalton Trans.* **2009**, 1080.
- (6) Faller, P. *ChemBioChem* **2009**, *10*, 2837.
- (7) Dorlet, P.; Gambarelli, S.; Faller, P.; Hureau, C. *Angew. Chem., Int. Ed.* **2009**, *48*, 9273–9276.
- (8) Hureau, C.; Coppel, Y.; Dorlet, P.; Solari, P. L.; Sayen, S.; Guillou, E.; Sabater, L.; Faller, P. *Angew. Chem., Int. Ed.* **2009**, *48*, 9522–9525.
- (9) Shin, B.-K.; Saxena, S. *Biochemistry* **2008**, *47*, 9117–9123.
- (10) Shin, B.-K.; Saxena, S. *J. Phys. Chem. B* **2011**, *115*, 15067–15078.
- (11) Drew, S. C.; Masters, C. L.; Barnham, K. J. *J. Am. Chem. Soc.* **2009**, *131*, 8760–8761.
- (12) Hou, L.; Zagorski, M. G. *J. Am. Chem. Soc.* **2006**, *128*, 9260–9261.
- (13) Azimi, S.; Rauk, A. *Int. J. Alzheimers Dis.* **2011**, *2011*, Article ID 539762, 15 pages. DOI: 10.4061/2011/539762
- (14) Atamna, H.; Frey, W. H., II; Ko, N. *Arch. Biochem. Biophys.* **2009**, *487*, 59–65.
- (15) Rowland, P.; Blaney, F. E.; Smyth, M. G.; Jones, J. J.; Leydon, V. R.; Oxbridge, A. K.; Lewis, C. J.; Tennant, M. G.; Modi, S.; Eggleston, D. S.; Chinery, R. J.; Bridges, Angela, M. *J. Biol. Chem.* **2006**, *281*, 7614–7622.
- (16) Nicholls, P.; Fita, I.; Loewen, P. C. *Adv. Inorg. Chem.* **2001**, *51*, 51–106.
- (17) Berglund, G. I.; Carlsson, G. H.; Smith, A. T.; Szöke, H.; Henriksen, A.; Hajdu, J. *Nature* **2002**, *417*, 463–468.
- (18) Gajhede, M. *Biochem. Soc. Trans.* **2001**, *29*, 91–99.
- (19) Wondimagegn, T.; Rauk, A. *J. Phys. Chem. B* **2011**, *115*, 569–579.
- (20) Wondimagegn, T.; Rauk, A. *J. Phys. Chem. B*, in press. <http://dx.doi.org/10.1021/jp305864y>.
- (21) Frisch, M. J.; Trucks, G. W.; Schlegel, H. B.; Scuseria, G. E.; Robb, M. A.; Cheeseman, J. R.; Scalmani, G.; Barone, V.; Mennucci, B.; Petersson, G. A.; Nakatsuji, H.; Caricato, M.; Li, X.; Hratchian, H. P.; Izmaylov, A. F.; Bloino, J.; Zheng, G.; Sonnenberg, J. L.; Hada, M.; Ehara, M. T.; Fukuda, R.; Hasegawa, J.; Ishida, M.; Nakajima, T.; Honda, Y.; Kitao, O.; Nakai, H.; Vreven, T.; Montgomery, J. A., Jr.; Peralta, J. E.; Ogliaro, F.; Bearpark, M.; Heyd, J. J.; Brothers, E.; Kudin, K. N.; Staroverov, V. N.; Kobayashi, R.; Normand, J.; Raghavachari, K.; Rendell, A.; Burant, J. C.; Iyengar, S. S.; Tomasi, J.; Cossi, M.; Rega, N.; Millam, N. J.; Klene, M.; Knox, J. E.; Cross, J. B.; Bakken, V.;

Adamo, C.; Jaramillo, J.; Gomperts, R.; Stratmann, R. E.; Yazyev, O.; Austin, A. J.; Cammi, R.; Pomelli, C.; Ochterski, J. W.; Martin, R. L.; Morokuma, K.; Zakrzewski, V. G.; Voth, G. A.; Salvador, P.; Dannenberg, J. J.; Dapprich, S.; Daniels, A. D.; Farkas, Ö.; Foresman, J. B.; Ortiz, J. V.; Cioslowski, J.; Fox, D. J. *Gaussian 09*, revision A.02; Gaussian, Inc.: Wallingford, CT, 2009.

(22) Cornell, W. D.; Cieplak, P.; Bayly, C. I.; Gould, I. R.; Merz, K. M., Jr.; Ferguson, D. M.; Spellmeyer, D. C.; Fox, T.; Caldwell, J. W.; Kollman, P. A. *J. Am. Chem. Soc.* **1995**, *117*, 5179–5197. <http://ambermd.org/> (accessed September 2012).

(23) Clemente, F.; Vreven, T.; Frisch, M. J. In *Quantum Biochemistry*; Matta, C., Ed.; Wiley VCH: New York, 2008.

(24) Vreven, T.; Morokuma, K. In *Continuum Solvation Models in Chemical Physics: From Theory to Applications*; Mennucci, B., Cammi, R., Eds.; Wiley: New York, 2008.

(25) Hertwig, R. H.; Koch, W. *Chem. Phys. Lett.* **1997**, *268*, 345–351.

(26) Scott, A. P.; Radom, L. *J. Phys. Chem. B* **1996**, *100*, 16502–16513.

(27) Tomasi, J.; Mennucci, B.; Cammi, R. *Chem. Rev.* **2005**, *105*, 2999–3093.

(28) Grimme, S.; Antony, J.; Ehrlich, S.; Krieg, H. *J. Chem. Phys.* **2010**, *132*, 154104–154122.

(29) Raffa, D. F.; Rauk, A. *J. Phys. Chem. B* **2007**, *111*, 3789–3799.

(30) Brault, D.; Rougee, M. *Biochem. Biophys. Res. Commun.* **1974**, *57*, 654–659.

(31) Al-Jaff, G.; Silver, J.; Wilson, M. T. *Inorg. Chim. Acta* **1990**, *176*, 307–316.

(32) Singh, R.; Grigg, J. C.; Armstrong, Z.; Murphy, M. E. P.; Eltis, J. D. *J. Biol. Chem.* **2012**, *267*, 10623–10630.

(33) Rozga, M.; Kloniecki, M.; Dadlez, M.; Bal, W. *Chem. Res. Toxicol.* **2010**, *23*, 336–340.

(34) Feaga, H. A.; Maduka, R. C.; Foster, M. N.; Szalai, V. A. *Inorg. Chem.* **2011**, *50*, 1614–1618.

(35) Shearer, J.; Szalai, V. A. *J. Am. Chem. Soc.* **2008**, *130*, 17826–17835.